

**Investigating the effect of rotor blade surface area
modifications on underwater turbine electrical generation**

Research Question: How does the rotor blade surface area (m^2) of an underwater turbine affect its efficiency in generating electrical power output (W)?

Word Count: 3995

Table of Contents:

1. Introduction.....	3
2. Background Information.....	5
2.1 Drag Forces.....	5
2.2 Turbine Energy Extraction and Betz Limit.....	7
2.3 Power Generation and Measurement.....	9
2.4 Analysis Method.....	9
3. Methodology.....	10
3.1 Justification for Set-Up.....	10
3.1.1 The System.....	10
3.1.2 The Pump.....	11
3.1.3 The Water Level.....	11
3.1.4 The Turbine.....	12
3.2 Variables.....	13
3.2.1 Independent Variables.....	13
3.2.2 Dependent Variables.....	14
3.2.3 Controlled Variables.....	14
3.3 Apparatus.....	17
3.4 Procedure.....	18
3.4.1 System Setup and Preparation.....	18
3.4.2 Initial Testing.....	19
3.4.3 Surface Area Modification and Data Collection.....	19
4. Data Analysis.....	21
4.1 Raw Data.....	21
4.2 Processed Data.....	21
4.3 Relative Efficiency Analysis.....	22
4.4 Theoretical Model and Experimental Data Comparison.....	24
4.5 Comparative Trend Analysis.....	26
5. Conclusion.....	28
5.1 Evaluation.....	30
5.1.1 Methodology Limitations.....	31
5.1.2 Theoretical Model Failure.....	32
5.1.3 Improvements for Future Work.....	32
5.1.4 Unresolved Questions.....	33
References.....	34

1. Introduction

Generating usable electrical power from natural energy sources is known as renewable energy generation, and it's one of the most challenging problems facing developing countries in the twenty-first century (Whba, 2025). As global energy demands continue to rise while traditional fossil fuel reserves diminish with every day, the urgent need for sustainable and locally implementable energy solutions has become increasingly popular (Licaj, 2022).

In the Central Asian countries, for example, in countries like Kyrgyzstan, where approximately 94% of the whole terrain consists of mountainous regions, there exist unique challenges for renewable energy implementation (*Visit Kyrgyz*, 2022). Compared to the wind turbines, which require enormous flat spaces and specially trained maintenance specialists, underwater turbines can utilize existing water systems such as rivers and irrigation channels (Hopkins, 2024). This benefit is especially evident in mountainous areas where topographical features frequently alter wind patterns, resulting in erratic turbulence and making the economic appeal of large-scale wind energy generation impractical (Dorminey, 2012).

My personal experience with energy shortages in Osh, a small town in the southern part of Kyrgyzstan, is what inspired me to conduct this research. The frequent power outages lasting several hours or even days have affected me and my communities. These disruptions, exacerbated by the ageing Soviet-era infrastructure, have prompted the government to implement household energy-limiting systems, including smart electricity controllers that automatically cut power when consumption exceeds 5 kW (JSC NEWK, 2024). While these measures are effective, they aren't sustainable in the long term. I believe that we should

develop small-scale renewable energy strategies that can be produced and maintained locally rather than relying entirely on foreign power plants.

The physics behind an underwater turbine involves complex interactions between fluid dynamics principles and electromagnetic induction of the motor. And water, being approximately 800 times denser than air, allows underwater turbines to generate significantly more energy than compared to wind turbines in the same conditions (Starr, 2021).

According to the Betz limit, there is no existing turbine that can capture more than 59.3% of the kinetic energy available from any fluid (Donev, 2024). However, this efficiency can be further affected, making the real limit even lower when taking into account other variables. The addition of fin-like attachments further affects its dynamics: greater surface area creates more area for momentum transfer from flowing water to rotating blades, but also increases total drag force acting against rotation. To better show the relationship between blade design and the electrical power generation, this study uses fin-like attachments on the rotor blades to vary the blade surface area while keeping water flow conditions constant.

The investigation addresses the research question: "*How does the surface area of the rotor blades on an underwater turbine impact its efficiency in generating electrical power?*" The goal is to experimentally determine the relationship between blade surface area and electrical power output while analyzing the physics principles behind and evaluating possible

applications for small-scale turbines in developing nations, where energy scarcity remains a critical concern.

2. Background Information

2.1 Drag Forces

When water flows through a submerged part, it exerts a drag force that opposes the motion (the flow of water). Unlike other resistive forces, drag forces depend on the velocity. Drag force is proportional to the squared velocity for a turbulent flow (Todreas, 2017). The drag force equation:

$$F_d = C_d A \frac{\rho V^2}{2} , \quad (1)$$

where F_d is a drag force (N), C_d is the drag coefficient, ρ is water density ($1,000 \text{ kg/m}^3$), A is the surface area (m^2), and v is the relative velocity between water and surface (m/s) (Todreas, 2017).

For the turbine blades, this drag force acts at 90° to oppose the rotation, as shown in Figure 1. As surface area, A , increases through the fin attachments, the total drag force increases proportionally.

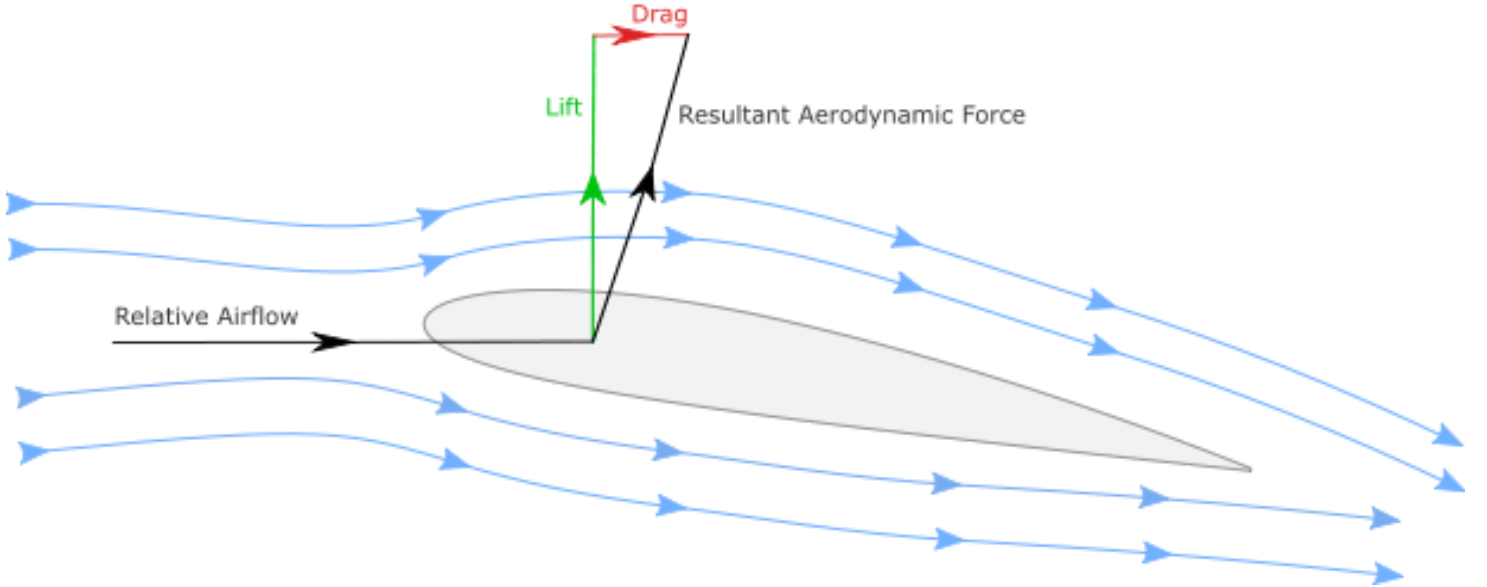


Figure 1: Diagram showing force vectors acting on the turbine

The key insight for this investigation is that **drag force is directly proportional to surface area** (from equation 1) when other factors remain constant. Therefore, the ratio between the modified and original configuration is:

$$\frac{F_{d, \text{modified}}}{F_{d, \text{original}}} = \frac{C_{d, \text{modified}} A_{\text{modified}}}{C_{d, \text{original}} A_{\text{original}}}, \quad (2)$$

Key Assumptions and Justification: for small object attachments such as fins with small surface area, the researches suggest that drag coefficient changes are typically non-noticeable. Other studies on real-world wind turbine blade modifications show that small surface attachments can change drag by 4-6%, while surface area increases are actually substantially bigger (Leonardo, 2013).

Simplified Approximation: for this investigation, we will assume $C_{d, \text{modified}} \approx C_{d, \text{original}}$, which simplifies equation (2) to:

$$\frac{F_{d, modified}}{F_{d, original}} = \frac{A_{modified}}{A_{original}}, \quad (3)$$

Where

- $F_{d, original}$: Total drag force acting on the original turbine blades (when 0 fins configuration) measured in Newtons (N)
- $F_{d, modified}$: Total drag force acting on the modified turbine blades (with n-fins attached) measured in Newtons (N)
- $A_{original}$: Total surface area of original turbine blades measured using Fusion360 CAD software (m^2)
- $A_{modified}$: Total surface area of modified turbine blades, including fin attachments, measured using Fusion360 CAD software (m^2)

This relationship allows for the prediction of the relative drag increases based on the measured surface area changes from the experimental data.

2.2 Turbine Energy Extraction and Betz Limit

Underwater turbines work by converting the kinetic energy of flowing water into rotational mechanical energy through hydrodynamic forces acting on the rotor blades. However, not all the energy from the water is converted into mechanical energy due to Betz's Law. This law states that no turbine can extract more than 16/27 (59.3%) of the kinetic energy from the fluid flowing through (Vennell, 2013). This means that the turbine usually falls short of this theoretical maximum limit.

Essentially, the Betz Limit is the maximum fraction of energy that can be taken from moving water (or air) without stopping it completely. **Figure 2**, below, helps explain this: as water

flows toward the turbine, it has some speed and energy. After passing through the turbine, the water still has to keep moving, or otherwise, new water could not flow in. This is why a turbine cannot capture 100% of the energy.

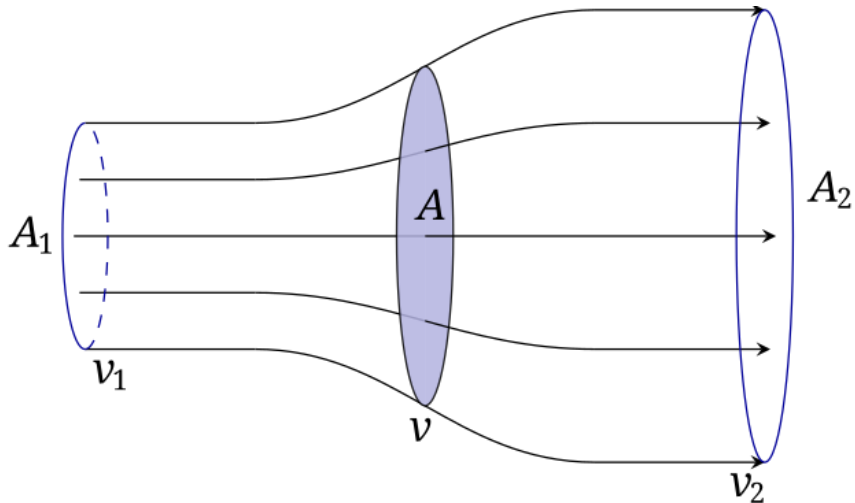


Figure 2: Schematic of fluid flow through a turbine (Bhaskara, 2015)

The shaded area marked "A" is the rotor swept area where the energy is extracted, while the flow before and after shows that some energy always remains in the moving stream. The number 59.3% comes from balancing how much the water slows down before and after the turbine. If it is slowed down too much, water wouldn't be able to keep flowing into the blades (Donev, 2024).

Thus, in practice, the extracted power is always multiplied by the coefficient of performance (C_p), which is limited by the Betz Limit. Real-world turbines achieve only 35-45% of the theoretical maximum due to various losses such as blade drag, mechanical friction, and uncontrolled flow conditions (Ragheb, 2011). Essentially, in this investigation, any increase in drag forces directly reduces the efficiency below even these real-world values.

2.3 Power Generation and Measurement

The DC motor acts as a generator in this investigation, turning rotational mechanical energy into electrical energy through electromagnetic induction. When rotated by an external source, the coil segments in the rotor rotate through a varying magnetic flux in the air gap (Portescap, 2021). Since the theoretical modeling with electromotive force (EMF) follows the relationship $\text{EMF} \propto \omega$ (where ω is the angular velocity), and we are unable to realistically calculate or estimate the angular velocity in the scope of this investigation, we will be measuring terminal voltage using a multimeter.

The EMF represents the motor's internal, ideal voltage, while the terminal voltage is the measurable voltage across the motor's GND and +. Although internal losses cause a small difference between the two, variations in EMF are also reflected in the terminal voltage proportionally (Tsokos, 2023).

The measurable electrical power output is:

$$P = V \times I = V^2/R, \quad (4)$$

where V is the terminal voltage measured by the multimeter and R is the known load resistance ($220 \pm 11 \Omega$). Thus, we don't need to measure the current and can derive it using Ohm's Law ($I = V/R$).

2.4 Analysis Method

Instead of calculating the absolute efficiency (which requires knowing the values of parameters such as water flow velocity, pump efficiency, and angular speed), this

investigation will use a relative efficiency analysis with the original (0-fins) configuration as the reference point.

Original Definition: $\eta_{relative}(0fins) = 100\% ,$ (5)

Modified Configuration Efficiency: $\eta_{relative}(n fins) = \frac{P_{n-fins}}{P_{0-fins}} \times 100\% ,$ (6)

where P is the power measured under identical flow conditions.

3. Methodology

3.1 Justification for Set-Up

3.1.1 The System

In this experiment, I used a set of plumbing tubes of different diameters to simulate underwater environments with a constant water flow rate. The turbine was placed in a 150mm diameter tube for free turbine movements. The system is placed horizontally, which results in the least energy loss during transition from Kinetic Energy (J) to the Mechanical Energy (J); skipping Potential Energy transformations. Built-in rubber and additional special tape were used between all tube connections, so no water is being leaked.



Figure 3: Complete experimental apparatus showing plumbing tube system with 150mm diameter testing section, circulation pump, and water level maintenance setup

3.1.2 The Pump

On the other end of the system, the water heater pump was placed. This exact pump is significantly cheaper, while generating the same amount of power (Watts), and thus more sustainable than other competitors. It creates just enough flow rate that let the motor spin. There are no other obstructions in the path of the water which may result in unpredictable speed changes.

3.1.3 The Water Level

On the other end of the system, the capillary tube is connected to maintain a constant water level at all times. This method ensures that if the water level drops even by the smallest measurement, the water from the connected bottle will rush into the system, until the chosen level is reached.

3.1.4 The Turbine

The propeller was 3D printed using ABS plastic, with 100% infill density. The design with 3 rotor blades was chosen due to the largest amount of surface area swept. Moreover, this design takes the least amount of time to produce on the 3D printer, while not requiring additional redundant supports, unlike other designs.

To change the surface area of the turbine sustainably, the option with rotor attachable fins was chosen, which successfully increases the turbine's surface area, without needing to reproduce different underwater turbines.

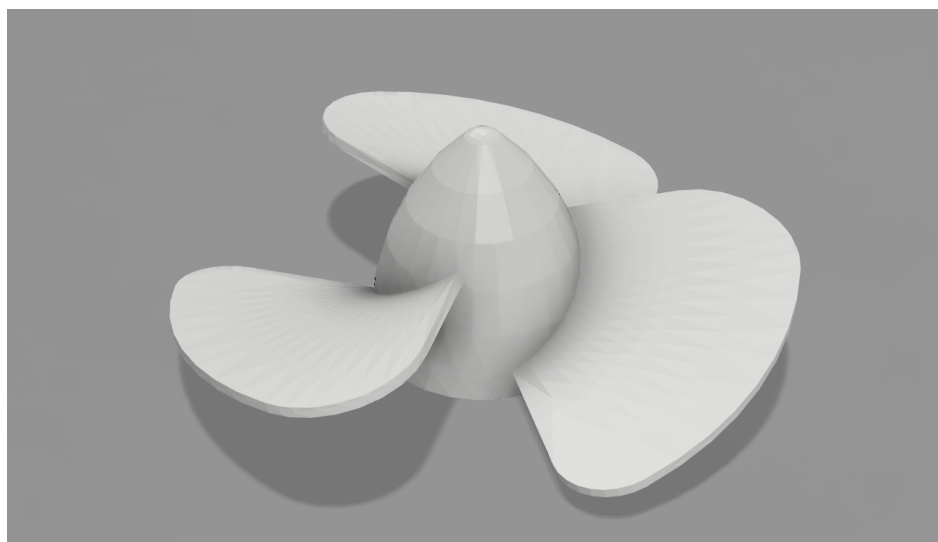


Figure 4: CAD model of baseline 3-rotor turbine design (0.0159 m² surface area) created in Fusion360

The chosen motor is a small DC motor, which was chosen primarily for its size and ability to continue working even in the water. While I covered the motor in the thermoplastic adhesive to reduce unnecessary vibrations and movements while in use, ensuring the turbine is aligned parallelly at all times. Another factor why it was chosen is due to its low voltage and current output values, which truly allow us to measure it accurately.



Figure 5: DC motor with waterproofing and turbine attachment, secured to minimize vibrations

3.2 Variables

3.2.1 Independent Variables

- 1. Surface Area of Rotor Blades (A):** this variable will be manipulated by attaching an even number of fins (0, 6, 12, 18 and 24), each fin with a surface area of 0.000295 m^2 , on the rotor blades while keeping the spacing equally distributed.



Figure 6: 3-rotor turbine design (0.0159 m^2 surface area) with fins attached in different configurations (0, 6, 12, 18, 24). Demonstrating the Independent Variable

3.2.2 Dependent Variables

The main dependent variable is the output power measured in watts using a digital multimeter. Further, the effect of the surface area on the efficiency of the underwater turbine relative to the potential power available from the water flow will be considered.

3.2.3 Controlled Variables

Table 1: Controlled Variables Table

Controlled Variables	Purpose	How was it controlled?
Rate of Water Flow	Different speeds of water will give unpredictable results each time. Ensures all trials are done in the same environment	Choose one pump setting for the entirety of the experiment
The Water Level	Inconsistent water levels will unpredictably affect the rate of water flow. It ensures all trials are done in the same environment	Attach a capillary system to maintain consistent water levels. Double-tape all the pipe connections to prevent leaks
The Motor	Different motors have different performance characteristics. Its components, mass, inertia, and resistance can affect its performance and efficiency	Use the same DC motor
The Motor Wire Type	Given that Resistance $R = \frac{\rho L}{A}$ is influenced by wire length (L), cross-area (A) and resistivity (ρ),	Use the same wire types when soldering extension wires to the motor

Controlled Variables	Purpose	How was it controlled?
	<p>using the same wire type ensures that the resistance stays constant, ensuring constant heat dissipation</p> $P = I^2R$	
Water Temperature	<p>Temperature affects water density and viscosity.</p> <p>Consistent water temperature ensures that fluid properties remain unchanged throughout the experiment</p>	<p>After each set of trials, change the water to the specially prepared water at a consistent temperature</p>
Turbine Position and Orientation	<p>The placement of the turbine relative to the water flow will be fixed (parallel) to avoid variations in the water flow distribution</p>	<p>Have specially prepared a non-movable attachment to the pipe, which keeps the turbine in a set position</p>

3.3 Apparatus

Table 2: Apparatus and Materials

Equipment	Specifications	Uncertainty	Purpose
UT33D+ Digital Multimeter	Voltage measurement	$\pm 0.1 * 10^{-2}$ V	Measure the electrical output voltage
220Ω Resistor	Store-bought resistor	$\pm 0.1 * 10^2$ Ω	Provide a consistent electrical load
XPS25-6-130B Circulation Pump	100W, 0.5A		Generate a constant water flow
3D printed Turbine Propeller	ABS plastic, 3 blades		Convert water flow to rotational motion
DC Motor	Small brushed motor		Generate electrical power from rotation
Plumbing Tubes	PVC Tube	± 1 mm	Navigate the water flow to the turbine
IV Drip Set	Medical level		Maintain a constant water level
Motor Mounting Bracket	Custom built		Secure motor position in the water flow

3.4 Procedure

3.4.1 System Setup and Preparation

Step 1: Pump assembly

The system of plumbing pipes was assembled horizontally using PVC pipes of varying diameters. A 150 mm diameter tube was positioned at the turbine to allow for free water flow movement. All pipes were sealed together using built-in rubber gaskets and additional waterproof Teflon tape to prevent further water leakage. The circulation pump of XPS25-6-130B model, 100W, 0.5A, was connected at one end of the system.

Step 2: Water level maintenance installation

A capillary IV drip set was connected to the opposite end of the main pipe system. A water bottle was attached to this IV drip set to maintain a constant water level throughout the entire investigation. The system was tested to ensure automatic water refuelling when levels dropped.

Step 3: Turbine and motor preparation

The 3D printed ABS plastic turbine propeller (with 100% infill density and 3 rotor blade design) was attached to the small DC motor shaft. The motor was then waterproofed using hot glue (although it works underwater) to prevent any water damage and reduce vibrations. This underwater turbine was placed parallel to the water flow direction within the 150 mm diameter testing tube.

Step 4: Electrical measurement setup

A UT33D+ multimeter was connected to the DC motor terminal wires. The multimeter was set to measure voltage (V), also a $(2.2 \pm 0.1) * 10^2 \Omega$ resistor was connected in series with the motor to provide an electrical load throughout all trials.

Step 5: Water temperature preparation

Specially prepared water was maintained at a constant temperature and kept ready in a separate container for use. This ensured consistent water temperatures and properties throughout the measurement trials.

3.4.2 Initial Testing

Step 6: Flow rate testing

The pump was activated and set to 100W power mode. The system was left to stabilize its flow conditions for about 5 minutes. Water flow rate consistency was verified by observing turbine rotation stability and ensuring no obstructions in the water flow path.

Step 7: Original measurements (0 fins configuration)

With no additional fins attached to the turbine blades, the original surface area was measured and recorded as 0.0159 m^2 on Fusion360. The turbine configuration consisted of three rotor blades with no surface area modifications.

3.4.3 Surface Area Modification and Data Collection

Step 8: Fin attachment procedure

For each subsequent trial, small shark-type fins were glued to the rotor blades in a balanced configuration. For each fin count level, fins were distributed equally across all three blades: if 6 fins total, then 2 fins per blade, 12 fins total, then 4 fins per blade, etc. Fins were positioned at equal distances from each other to not overload the rotor blade and attempt to reach the best fluid dynamics on the surface of the turbine.

Step 9: Surface area measurement

After each fin was installed, the total area was calculated by summing the original blade area plus the additional surface area contributed by the attached fins and subtracting the bottom of the fins.

Step 10: Data collection procedure

For each surface area configuration (0, 6, 12, 18, and 24 fins):

- a) The pump was activated at 100W power mode
- b) The system was left to stabilize for 1.5 minutes after powering on
- c) This stabilization process was repeated each time for the new set of trials
- d) Three separate voltage measurements were recorded afterwards, with 10-second intervals between each measurement
- e) Current (I) values were derived using Ohm's law ($I = V/R$) with the known resistor of $(2.2 \pm 0.1) * 10^2 \Omega$

Step 11: Water temperature control

After completing the 3 trial measurements each time for the new surface area configuration, all water was completely poured out of the system. The system was then refilled with prepared water of a constant temperature. This process ensured consistent water temperature and properties throughout all experimental trials.

Step 12: Fin modification between configurations

While water was being refuelled for the new surface area configuration, the turbine was detached to attach a new fin configuration. Then, the fins were repositioned or added depending on the configuration, and the turbine was placed back

4. Data Analysis

4.1 Raw Data

Table 3: Experimental Data

		Voltage (V) ± 0.003			
Configuration		Surface Area (m²) ± 0.000000025	Trial 1	Trial 2	Trial 3
0 fins		0.0159	0.193	0.205	0.195
6 fins		0.0166	0.136	0.123	0.131
12 fins		0.0173	0.109	0.103	0.112
18 fins		0.0180	0.092	0.087	0.098
24 fins		0.0187	0.074	0.069	0.062

4.2 Processed Data

Table 4: Processed Data and Calculation of Power and Mean Voltage

		Voltage (V) ± 0.003			Calculated Values		
Configuration		Trial 1	Trial 2	Trial 3	Mean Voltage (V)	Calculated Power (W)	Power Uncertainty (W)
0 fins	0.0159	0.193	0.205	0.195	0.198 ± 0.007	1.8×10^{-4}	$\pm 0.2 \times 10^{-4}$
6 fins	0.0166	0.136	0.123	0.131	0.130 ± 0.007	7.7×10^{-5}	$\pm 1.3 \times 10^{-5}$
12 fins	0.0173	0.109	0.103	0.112	0.108 ± 0.005	5.3×10^{-5}	$\pm 0.8 \times 10^{-5}$
18 fins	0.0180	0.092	0.087	0.098	0.0923 ± 0.006	3.9×10^{-5}	$\pm 0.7 \times 10^{-5}$
24 fins	0.0187	0.074	0.069	0.062	0.0683 ± 0.006	2.1×10^{-5}	$\pm 0.6 \times 10^{-5}$

The experimental data collected from the underwater turbine are presented in Table 4, above, showing voltage measurements for each surface area configuration. Using the relationship $P = V^2/R$ from equation (4), where $R = (2.2 \pm 0.1) * 10^2 \Omega$.

Sample Power Calculation for 0 Fins Configuration: $P = V^2/R = (0.198)^2/(220) = 1.78 \times 10^{-4} \text{ W}$

Uncertainty Analysis: The uncertainty for electrical power is calculated as follows:

$$\frac{\Delta P}{P} = 2\left(\frac{\Delta V}{V}\right) + \left(\frac{\Delta R}{R}\right), \quad (7)$$

4.3 Relative Efficiency Analysis

Following the methodology outlined in section 2.4, relative efficiency was calculated using the 0-fins configuration as the reference point (100% efficiency). The relationship used was from equation (6):

$$\eta_{relative}(n \text{ fins}) = \frac{P_{n-fins}}{P_{0-fins}} \times 100\% \quad (6)$$

Table 5: Relative Efficiency Calculations

Configuration	Surface Area Ratio	Calculated Power (W)	Relative Efficiency (%)	Efficiency Uncertainty (%)
0 fins	1.00	1.8×10^{-4}	1.0×10^2	$\pm 0.1 \times 10^2$
6 fins	1.04	7.7×10^{-5}	0.4×10^2	$\pm 0.1 \times 10^2$
12 fins	1.09	5.3×10^{-5}	0.3×10^1	$\pm 0.9 \times 10^1$
18 fins	1.13	3.9×10^{-5}	0.2×10^1	$\pm 0.9 \times 10^1$
24 fins	1.18	2.1×10^{-5}	0.1×10^1	$\pm 0.8 \times 10^1$

The results from Table 5 demonstrate a strong negative correlation between the increase in surface area and electrical power generation efficiency. The addition of 24 fins resulted in an 88.1% decrease in relative efficiency, despite only a 17.6% increase in total surface area. In physical terms, increased surface area raises the drag force (equation 1), which opposes rotation, reducing angular velocity and consequently decreasing electromagnetic induction in the DC motor, producing lower voltage and power output.

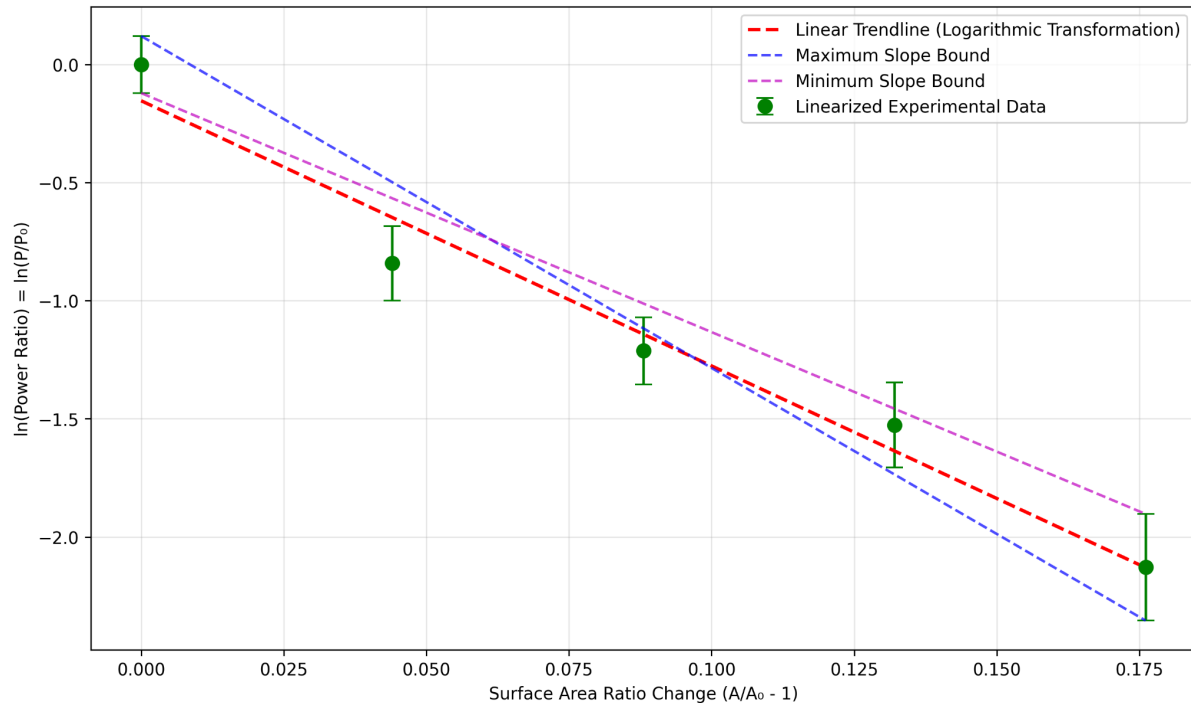


Figure 7: Graph showing relative efficiency (%) versus surface area ratio change ($A/A_0 - 1$), with error bars representing uncertainties

Figure 7 shows the logarithmic transformation of the power ratio data, which converts the exponential relationship into a linear one. Taking the natural logarithm of P/P_0 and plotting it against $(A/A_0 - 1)$ produces a straight line, proving that the exponential model

$$P/P_0 = e^{-k(\frac{A}{A_0} - 1)}$$

is correct. The linear fit has a strong correlation, and the slope of this line

equals $-k$ (the decay coefficient). The two dashed uncertainty bound lines show the maximum and minimum possible slopes based on dashed error bars connecting the highest point of the first data point to the lowest point of the last data point (and vice versa).

Negative y-values simply mean the power ratio P/P_0 is less than 1. Since $\ln(1) = 0$, any ratio below 1 gives a negative logarithm. All configurations with fins generated less power than the 0-fins baseline, so all $\ln(P/P_0)$ values are negative.

4.4 Theoretical Model and Experimental Data Comparison

Based on the drag force analysis from section 2.1, we can make theoretical predictions about how surface area changes should affect power output. The comparison tests whether our simplified drag model accurately describes the real physics.

Drag Force Prediction

From equation (3):

$$\frac{F_{d, \text{modified}}}{F_{d, \text{original}}} = \frac{A_{\text{modified}}}{A_{\text{original}}}, \quad (3)$$

we can see that if the surface area increases by 4.4% (6 fins), the drag force should increase by 4.4%.

Power Reduction Prediction

For small increases in drag force, we expect small decreases in rotational speed, leading to small decreases in voltage and power. If drag increases by 4.4%, power should decrease by approximately 4.4%.

Therefore: *Theoretical Power Ratio = 1 / (Surface Area Ratio)*

Calculation Example:

- 6 fins: Surface area ratio = 1.044
- Predicted drag increase = 4.4%
- **Theoretical** power ratio = 1/1.044 = 0.958 (4.2% power decrease)
- **Experimental** power ratio = 0.432 (56.8% power decrease)

Table 6: Theoretical vs Experimental Comparison

Configuration	Surface Area Ratio	Theoretical Power Ratio	Experimental Power Ratio
0 fins	1.00	1.00	1.00
6 fins	1.04	0.958	0.432
12 fins	1.09	0.919	0.298
18 fins	1.13	0.883	0.217
24 fins	1.18	0.850	0.119

The experimental power ratios deviated significantly from theoretical predictions based on simple drag equations (see Section 6 for detailed comparison), suggesting complex fluid dynamic effects beyond the scope of equation (1).

4.5 Comparative Trend Analysis

While the experimental values differ significantly from theoretical predictions, we can analyze whether the rate of decline follows similar patterns by comparing how quickly power decreases as surface area increases in both experimental and theoretical cases.

For experimental data, this exponential mathematical equation is chosen:

$$\frac{P}{P_o} = e^{-k(\frac{A}{A_o} - 1)}, \quad (8)$$

For the theoretical model, this linear mathematical equation is chosen:

$$\frac{P}{P_o} = \frac{1}{\frac{A}{A_o}}, \quad (9)$$

This equation (8) was chosen because it directly suits the experimental data values, and it shows a curved decline when plotted. The equation (9) was directly derived from the theoretical assumption of equation (3). If $F_d \propto A$ (equation 3), then the drag force increases linearly with surface area.

Even if absolute values differ, similar decline rates would suggest the same underlying physics mechanisms. Different decline rates indicate fundamentally different physical processes.

To fairly compare the decline coefficients, we will use the same exponential equation (8) for the theoretical model as well. And we will use logarithms to find k (the decline coefficient).

Table 7: Decline Coefficient Comparison

Model Type	Decline Coefficient (k)	R ² Value	Physical Interpretation
Experimental Data	$k_{exp} = 14.4 \pm 1.5$	0.966	Huge exponential decline due to the complex fluid effects
Theoretical Data	$k_{theory} = 0.93 \pm 0.01$	0.999	Slight exponential decline from our theoretical model
Ratio (k_{exp} / k_{theory})	15.5	-	Experimental decline 15x steeper than predicted

The R² is a statistical measure that tells you how well your mathematical model fits your experimental data (Fernando, 2019). The formula to calculate is:

$$R^2 = 1 - \frac{SS_{res}}{SS_{tot}}, \quad (11)$$

where:

- SS_{res} = Sum of squared differences between your data points and the fitted line
- SS_{tot} = Sum of squared differences between your data points and their average
(Nagelkerke, 1991)

The 15x difference in decline coefficients proves that fins don't just add drag, they trigger some fluid dynamic effects (turbulence, flow separation, wake interference) that create exponentially worse performance degradation than simple drag theory can predict.

5. Conclusion

This investigation directly answers the research question that increasing rotor blade surface area causes electrical power output to decrease exponentially. The mathematical relationship is

$$\frac{P}{P_0} = e^{(-14.4(\frac{A}{A_o} - 1))}, \quad (12)$$

with $R^2 = 0.966$, which means the model fits the experimental data really well.

When surface area increased by 18% (from 0.0159 m^2 to 0.0187 m^2), electrical power dropped by 88.1% (from $1.8 \times 10^{-4} \text{ W}$ to $2.1 \times 10^{-5} \text{ W}$). This massive drop confirms the hypothesis from Section 2 that "increasing surface area will increase drag forces and ultimately decrease power generated".

But here's where it gets interesting. The theoretical drag model from Section 2.1 only predicted 4-15% power decreases based on equation (3). The actual experiment showed 57-88% losses. The experimental decline coefficient ($k_{\text{experimental}} = 14.4 \pm 1.53$) ended up being 15 times larger than what theory predicted ($k_{\text{theory}} = 0.93 \pm 0.01$). This huge gap means that adding fins doesn't just increase drag in a simple, predictable way. The fins actually create turbulence, flow separation, and wake interference that make everything much worse than basic drag equations would suggest.

Despite measurement uncertainties of 7.8-11.8%, the exponential relationship ($R^2 = 0.966$) confirms that surface area modifications drastically reduce power output. This explains why real turbines use streamlined blades. At low water speeds, drag forces dominate and reduce efficiency far below the practical 35-45% of the Betz limit.

For small-scale turbine applications in places like Kyrgyzstan, the takeaway is straightforward: keep blade surfaces smooth and don't add surface area. Any rough surfaces or attachments will kill power generation at the low water speeds you find in small rivers and irrigation channels.

Future work should test this relationship at different water velocities (0.5-2.0 m/s) to see if there's a speed where increased surface area might actually help. Different fin shapes could also be tested to figure out which creates less turbulence. Measuring angular velocity directly with a tachometer would let you calculate absolute efficiency instead of just relative efficiency, which would make the results easier to compare with industrial turbine data. This experiment showed that adding surface area reduces power generation exponentially. The 15 \times difference between theory and experiment demonstrates that real fluid dynamics is

more complex than basic equations predict, highlighting why experimental testing is essential in engineering design.

5.1 Evaluation

Table 7 summarizes systematic and random uncertainties:

Table 8: Uncertainty analysis table

Systematic Uncertainties		Random Uncertainties	
Voltage measurement precision	$\pm 0.1 * 10^{-1}$ V multimeter uncertainty adds 3.6-14.6% to power uncertainty, depending on voltage magnitude	Flow variations	Although the pump setting was constant, minor turbulence might have affected the flow.
Resistor tolerance	$\pm 0.1 * 10^2 \Omega$ contributes 5.0% to all power calculations	Temperature effects	Water temperature changes could affect motor resistance and fluid properties
Surface area measurements	CAD (software) measurement precision estimated at $\pm 2\%$ of the total surface area	Alignment variations	The turbine was inevitably slightly changed in position between trials

The combined power uncertainty ranged from 7.8% to 11.8%. Lower voltages had worse signal-to-noise ratios - at 24 fins (0.0683 V), the measurement uncertainty represented 14.6% of the power, while at 0 fins (0.198 V) it was only 3.6%. This is visible in Figure 6 (below), where error bars are larger for configurations with more fins.

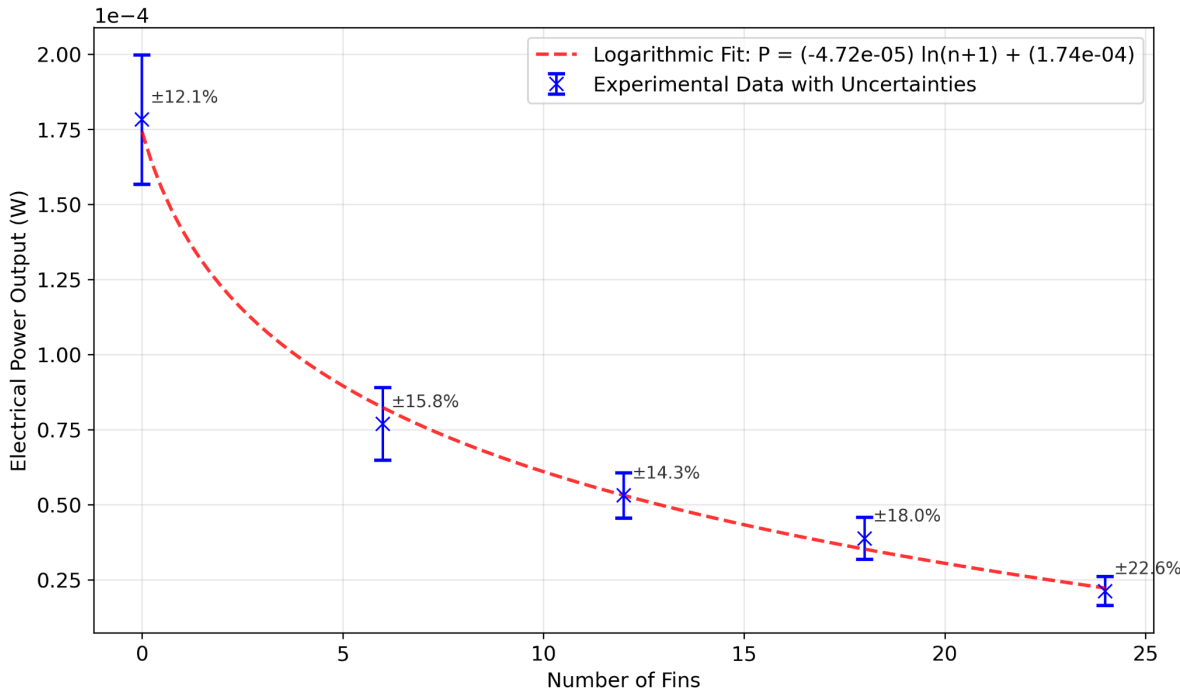


Figure 6: Error bar analysis showing how uncertainties vary across different fin configurations

Despite these uncertainties, the exponential model with $R^2 = 0.966$ proves the relationship is real. Even if all errors combined in the worst direction ($\pm 12\%$), this can't explain the $15\times$ difference between theory and experiment. That gap represents actual physics, not measurement noise.

5.1.1 Methodology Limitations

The biggest limitation was testing only one water velocity. The exponential relationship ($k_{\text{experimental}} = 14.4$) only applies to this low-speed regime. At higher velocities, the relationship might be completely different. Without a flow meter, the exact speed is unknown (estimated 0.3-0.5 m/s based on observation).

Using relative efficiency instead of absolute efficiency was practical but limited. Without measuring angular velocity directly, the actual mechanical-to-electrical conversion efficiency remains unknown, making it impossible to compare with published turbine data.

Glueing fins onto blades isn't how real turbines are designed. The hot glue added mass and created rough surfaces at attachment points. Each fin edge caused flow separation and turbulence. Professional turbines have smooth, integrated designs manufactured as single pieces.

5.1.2 Theoretical Model Failure

Section 2.1 assumed the drag coefficient stayed constant $C_{d, modified} \approx C_{d, original}$, which turned out to be completely wrong. The theory predicted 4-15% power decreases, but experiments showed 57-88% losses. This 15 \times gap happened because fins didn't just add surface area - they created turbulence, flow separation, and wake interference that the simple equation 1 can't predict. This is actually the investigation's most important finding: real fluid dynamics is far more complex than textbook models suggest.

5.1.3 Improvements for Future Work

Three key improvements would strengthen the investigation:

1. Install a flow meter to measure actual water velocity and test at multiple speeds (0.5, 1.0, 1.5, 2.0 m/s) to see if $k_{experimental}$ changes with velocity
2. Use a tachometer to measure rotation speed directly, allowing absolute efficiency calculations
3. 3D print integrated blade designs instead of glueing fins, eliminating mass and surface roughness issues

5.1.4 Unresolved Questions

Several questions remain: At what velocity would increased surface area start helping instead of hurting? What's the optimal surface area for this flow rate? How do streamlined fins compare to bluff rectangular fins? How do these findings scale to full-size turbines? The investigation successfully identified the exponential relationship at low speeds, but the limitations show where more research is needed. The gap between simple theory and experimental reality proves that fluid dynamics experiments are essential - textbook equations can't predict everything.

References

Bhaskara. (2015, March 20). *Betz Tube*. Betz Tube. Retrieved August 20, 2025, from

<https://commons.wikimedia.org/wiki/File:Betz-tube.svg>

Blazej, O. (2011). *TIDAL POWER SYSTEMS*. Description of Tidal Technology. Retrieved August

20, 2025, from

http://www.i15.p.lodz.pl/strony/EIC/res/Description_of_technology_tidal.html

Bobbitt, Z. (2020, April 24). *What is a Good R-squared Value?* What is a Good R-squared

Value? Retrieved August 30, 2025, from

<https://www.statology.org/good-r-squared-value/>

Donev, J. (2024). *Betz limit*. Energy Education. Retrieved June 29, 2025, from

https://energyeducation.ca/encyclopedia/Betz_limit

Dorminey, B. (2012, July 19). *Should the Wind Turbine Industry Head for the Hills?* Should the

Wind Turbine Industry Head for the Hills? Retrieved June 28, 2025, from

<https://www.renewableenergyworld.com/wind-power/turbines-equipment/should-the-wind-turbine-industry-head-for-the-hills/>

Dourmashkin, P. (2016). *8.6: Drag Forces in Fluids*. Physics LibreTexts. Retrieved August 20,

2025, from

[https://phys.libretexts.org/Bookshelves/Classical_Mechanics/Classical_Mechanics_\(Dourmashkin\)/08:_Applications_of_Newtons_Second_Law/8.06:_Drag_Forces_in_Fluids](https://phys.libretexts.org/Bookshelves/Classical_Mechanics/Classical_Mechanics_(Dourmashkin)/08:_Applications_of_Newtons_Second_Law/8.06:_Drag_Forces_in_Fluids)

Fernando, J. (2019). *R-Squared: Definition, Calculation, and Interpretation*. Investopedia.

Retrieved August 30, 2025, from

<https://www.investopedia.com/terms/r/r-squared.asp>

Gagnon, I. (2018, March 18). *Tidal Power (Based on the Numbers)*. Tidal Power (Based on the

Numbers). Retrieved 08 20, 2025, from

<https://www.linkedin.com/pulse/tidal-power-based-numbers-ian-gagnon>

H., Z. (2019). *SNR Estimate*. NMR Facility, UCSB Chem and Biochem. Retrieved August 30,

2025, from <https://nmr.chem.ucsb.edu/protocols/SNR.html>

Hopkins, E. (2024, October 1). *What Is Tidal Energy? How Do Tidal Turbines Generate*

Electricity? National Energy Foundation. Retrieved June 28, 2025, from

<https://nef.org.uk/what-is-a-tidal-turbine-and-how-does-it-generate-electricity-2/>

JSC NEWK. (2024, September 30). ОАО «Национальная электрическая сеть Кыргызстана»

завершило установку умных счетчиков в 10 РЭСах по республике. ОАО

«Национальная электрическая сеть Кыргызстана» завершило установку умных

счетчиков в 10 РЭСах по республике. Retrieved June 28, 2025, from

<https://nesk.kg/ru/press-centr/novosti-i-press-relizy/oao-nacionalnaya-elektrichesk>

aya-set-kyrgyzstana-zavershilo-ustanovku-umnyh-schetchikov-v-10-resah-po-respu

blike/

Leonardo, C., Roger, A., & Fotis, S. (2013, February 1). Drag reduction of large wind turbine

blades through riblets: Evaluation of riblet geometry and application strategies.

Renewable Energy, 50, 1095-1105. 10.1016/j.renene.2012.09.001

Licaj, E. (2022, July 6). *Are underwater turbines the next big clean energy source?* The World

Economic Forum. Retrieved June 28, 2025, from

<https://www.weforum.org/stories/2022/07/underwater-turbine-technology-clean-energy-source/>

Mycek, P., Gaurier, B., Germain, G., Pinon, G., & Rivoalen, E. (2014). *Experimental study of the turbulence intensity effects on marine current turbines behaviour. Part I: One single turbine*, (Vol. 66). Renewable Energy. <https://doi.org/10.1016/j.renene.2013.12.036>.

Nagelkerke, N. J. D. (1991). *A Note on a General Definition of the Coefficient of Determination* (3rd ed., Vol. 78). 10.1093/biomet/78.3.691

Nave, C. R. (2005). *Fluid Potential Energy*. HyperPhysics. Retrieved August 20, 2025, from <http://hyperphysics.phy-astr.gsu.edu/hbase/press.html>

Nave, C. R. (2005). *Pressure*. HyperPhysics Concepts. Retrieved August 20, 2025, from <http://hyperphysics.phy-astr.gsu.edu/hbase/pfric2.html#fke>

Portescap. (2021, December). *Running a Brushed DC Motor as a Generator*. Portescap. Retrieved August 21, 2025, from

<https://www.portescap.com/en/newsroom/whitepapers/2021/12/running-a-brushed-dc-motor-as-a-generator>

Ragheb, M. (2011). *Wind Turbines Theory - The Betz Equation and Optimal Rotor Tip Speed Ratio* (R. Carriveau, Ed.; Rupp Carriveau ed., Vol. 2). IntechOpen. 10.5772/21398

Starr, A. (2021, September 16). *Tidal Energy | PNNL*. Pacific Northwest National Laboratory. Retrieved June 28, 2025, from <https://www.pnnl.gov/explainer-articles/tidal-energy>

Todreas, N. (2017, December). *Drag Force - Drag Equation | Definition | nuclear-power.com*. Nuclear Power. Retrieved August 20, 2025, from

<https://www.nuclear-power.com/nuclear-engineering/fluid-dynamics/what-is-drag-air-and-fluid-resistance/drag-force-drag-equation/>

Tsokos, K. A. (2023). *Physics for the IB Diploma Coursebook with Digital Access (2 Years)*. Cambridge University Press.

Vennell, R. (2013). *Exceeding the Betz limit with tidal turbines* (Vol. 55). Renewable Energy.
<https://doi.org/10.1016/j.renene.2012.12.016>

Visit Kyrgyz. (2022). Visit Kyrgyz. Retrieved June 28, 2025, from
<https://www.visitkyrgyz.com/infodesk/geographical-facts>

Whba, R. (2025). *Renewable Energy Technologies and Strategies in the Global Energy Transition* (M. S. Suâe(tm)ait, H. Jarimi, & S. A. M. Noor, Eds.; Vol. 1499). American Chemical Society. <https://pubs.acs.org/doi/abs/10.1021/bk-2025-1499.ch002>